RATE AND TEMPERATURE DEPENDENT PLASTICITY AND FAILURE OF AA7017-T73: EXPERIMENTS AND MODELLING

M.J. Pérez-Martín[1*], B. Erice[2], F. Gálvez[1]

[1]Departamento de Ciencia de Materiales. E.T.S.I. Caminos, Canales y Puertos. Universidad Politécnica de Madrid. Calle Profesor Aranguren, s/n, 28040, Madrid, España
[2]Department of Mechanical and Process Engineering. Swiss Federal Institute of Technology (ETH). Technoparkstrasse, 1, 8005, Zurich, Switzerland
[*] E-mail: mariajesus.perez@mater.upm.es

RESUMEN

En esta investigación se presenta el modelo de plasticidad utilizado para describir el comportamiento de la aleación de aluminio 7017-T73 bajo cargas uniaxiales. Para ello, se ha realizado una serie de ensayos de tracción uniaxial a diferentes velocidades de deformación con probetas mecanizadas en varias orientaciones con respecto a la dirección de laminación del material. Los resultados experimentales revelan que la AA7017-T73 presenta un alto grado de anisotropía tanto en el límite elástico como en el flujo plástico. También, cabe destacar que el material presenta muy poca sensibilidad a la velocidad de deformación. Además, la AA7017-T73 presenta deformaciones de rotura muy diferentes para cada orientación de carga. A la vista de los resultados experimentales obtenidos, para describir el comportamiento observado del material se emplea la función de plastificación Yld2000-3d con endurecimiento por deformación tipo Voce. Las simulaciones por elementos finitos muestran que el modelo de plasticidad utilizado es capaz de describir con precisión las respuestas local y global del material bajo cargas uniaxiales. Por último, se presenta el criterio de rotura Cockcroft-Latham para describir el comportamiento a fractura anisótropo de la AA7017-T73.

PALABRAS CLAVE: Plasticidad, metales para blindaje, velocidad de deformación, fractura anisótropa.

ABSTRACT

A series of tensile tests on uniaxial specimens machined from different orientations with respect to the rolling direction was carried out at a wide range of loading rates for an aluminium 7017-T73 alloy. The experimental results revealed a high degree of anisotropy on both yield stress and plastic flow. In addition, the material showed very little strain-rate sensitivity. The measured fracture strains for different loading orientations showed large differences. In order to describe the material behaviour, the Yld2000-3d yield criterion and an isotropic Voce hardening model were used to describe the plasticity of the AA7017-T73. Finite element simulations showed that the plasticity model provided accurate predictions of local and global material responses under uniaxial loading. A Cockcroft-Latham failure criterion was presented for describing the anisotropic fracture behaviour of the AA7017-T73.

KEYWORDS: Plasticity, armour metals, loading rate, anisotropic fracture.

1. INTRODUCTION

Sheet metals, and particularly aluminium alloys, are prone to exhibit anisotropic mechanical behaviour. Because of the manufacturing processes, the material obtains a highly textured microstructure which is translated into a direction-dependent mechanical behaviour.

Various yield functions have been proposed over the years to describe the anisotropy of metallic sheets. Moreover, this choice typically depends on the material type; being Hill´s anisotropic plasticity model family the classical choice for steel and Barlat´s yield function family the most extended when using aluminium alloys. In order to accurately describe both yielding and plastic flow behaviour of sheet metals, the coefficients of the anisotropic yield functions commonly need to be optimized explicitly or iteratively from experimental tensile, shear or biaxial yield stresses and Lankford coefficients.

The Yld2000-2d yield criterion [1] has been widely employed to describe the yield surface of different aluminium alloys. However, in most mechanical problems full 3d analysis is needed. In the present work, an extension of the Yld2000-2d yield function for general three-dimensional stress states [2] and a Voce hardening model are used to describe the anisotropic plastic yielding of AA7017-T73 sheets.

2. EXPERIMENTS

The experimental program included the tensile testing of AA7017-T73 sheet specimens under uniaxial loading at three different strain rates and temperatures. Figure 1 shows the geometry of the specimens used for such experiments.
In all tests a random black speckle pattern on a thin layer of white matt paint was applied to the specimen surface in order to measure the surface displacements through Vic2D digital image correlation software from Correlated Solutions.

2.1. Material

Although a regular AA7017 is considered a medium-strength aluminium alloy, because of the T73 heat-treatment the AA7017-T73 is considered one of the highest-strength commercial aluminium alloys. It contains zinc as the primary alloying element, magnesium and chromium in a lesser proportion. Magnesium produces a marked improvement in precipitation hardening characteristics, whereas chromium provides an increase of the stress corrosion cracking resistance. The detailed chemical composition in weight percentage is presented in Table 1. The alloy is solution heat-treated with an artificial aging. This T73 heat-treatment leaves the alloy beyond the point of maximum strength and achieves the best stress corrosion resistance.

2.2. Quasi-static experiments

Low strain rate experiments were carried out on a MTS hydraulic testing machine at a crosshead displacement of 0.6 mm/min. The material was tested under uniaxial loading along three different directions (0º, 45º and 90º), being 0º the rolling direction and 90º the transverse direction. An AVT Pike F-505B/C camera was set to record 2 fps with a resolution of 2452 x 2052 pixels. The experiments were carried out at room temperature and 75ºC.

2.3. Intermediate strain rate experiments

Intermediate strain rate experiments were carried out on the same hydraulic testing machine as the previous tests but at a crosshead displacement of 600 mm/min. In this case, a Phantom 7.3 high speed camera took 1000 fps with a resolution of 800 x 456 pixels. The image acquisition was triggered by the rise in the force signal recorded by the load-cell.

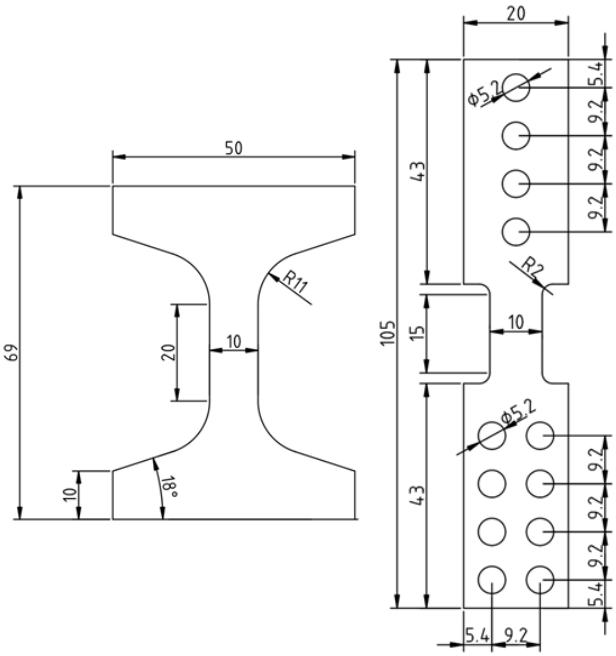

Figure 1. 1 mm thick specimens used for the experiments at low and intermediate strain rates on the left, and at high strain rates on the right.

2.4. High strain rate experiments

A Split-Hopkinson Pressure Bar (SHPB) set-up equipped with a custom-made load-inversion device [3]. was used to carry out the experiments at high strain rates The system (see Figure 2) comprised of a striker, an input bar, a load-inversion device and an output bar, with the latter positioned on top of the input bar. The load-inversion device consisted of a pusher, which inverted the incoming compressive pulse from the input bar into a tensile loading of the specimen. The opposite grip section of the specimen fitted into a machined slit in the output bar, which was closed by counter-sunk screws, thus maintaining a symmetric mass distribution with respect to the output bar's centre axis. The assembly was guided through bearings with lubricated contact surfaces. A strain gauge positioned at a distance of 320 mm from the specimen/output bar interface was used to record the output bar strain history $\varepsilon_t(t)$. The axial force acting on the specimen was then calculated as:

$$F(t) = E_b A_b \varepsilon_t(t) \tag{1}$$

where E_b and A_b are the elastic modulus and cross-section area of the output bar. For the displacement measurements, the same high speed camera as for the intermediate strain rate experiments was employed. The camera was set to an acquisition rate of 160000 fps at 432 x 32 pixels, being the interval between images 6.25 μs. The camera was triggered when the input bar strain gauge detected the rising edge of the incident wave.

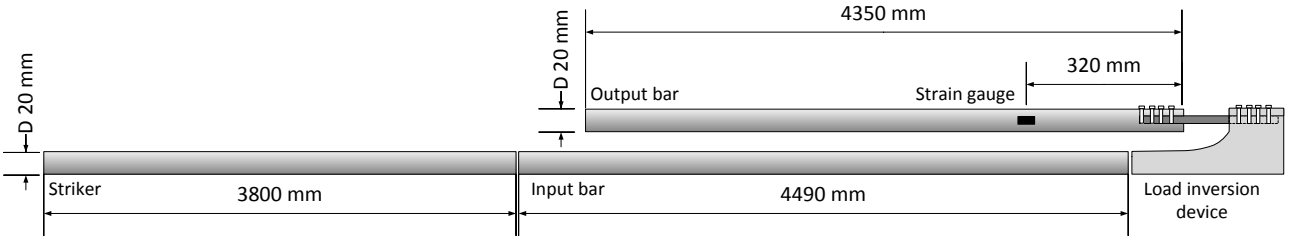

Figure 2. Illustration of the SHPB set-up in conjunction with the load-inversion device.

Table 1. Chemical composition in weight percentage of the AA7017-T73.

Zn	Mg	Fe	Si	Cu	Mn	Cr	Zr
5.1	2.4	0.3	0.16	0.12	0.22	0.16	0.12

2.5. Results

The engineering stress-strain curves corresponding to the quasi-static tests 0º (black), 45º (blue) and 90º (green) are shown in Figure 3. The figure clearly shows the anisotropy of the material. Such anisotropy could be described quantitatively by the Lankford coefficients (r-values) and the yield stresses corresponding to the 0º, 45º and 90º orientations. Based on the assumption of plastic incompressibility, the r-values were then determined from the ratios of the in-plane over the through-thickness logarithmic plastic strains, $r_\theta = \varepsilon_p^w / \varepsilon_p^t$ where θ is the direction of a vector aligned with the loading axis with respect to the rolling direction. The obtained uniaxial yield stresses Y_0, Y_{45}, Y_{90}, and Lankford coefficients r_0 r_{45}, r_{90}, are summarized in Table 2. The results showed that the AA7017-T73 was anisotropic both in strength and plastic flow.

Figure 4 shows the experimental engineering stress-strain response of the specimens oriented at 0º with increasing loading rates. The quasi-static experiments at $5{\cdot}10^{-4}$ s^{-1} are plotted in black, the intermediate strain rate test performed at 0.5 s^{-1} are shown in blue, and the dynamic stress-strain response of the material at 250 s^{-1} is depicted in green. As expected, there was almost no strain-rate sensitivity.

3. CONSTITUTIVE MODELLING

3.1. Constitutive equations

Being $\boldsymbol{\varepsilon} = \{\varepsilon_{xx} \quad \varepsilon_{yy} \quad \varepsilon_{zz} \quad 2\varepsilon_{xy} \quad 2\varepsilon_{yz} \quad 2\varepsilon_{xz}\}^T$ the vector form of the strain tensor and assuming the additive decomposition of the strain tensor $\boldsymbol{\varepsilon} = \boldsymbol{\varepsilon}^e + \boldsymbol{\varepsilon}^p$, its elastic part and the vector form of the Cauchy stress tensor $\boldsymbol{\sigma} = \{\sigma_{xx} \quad \sigma_{yy} \quad \sigma_{zz} \quad \sigma_{xy} \quad \sigma_{yz} \quad \sigma_{xz}\}^T$ are related as follows:

$$\boldsymbol{\sigma} = \boldsymbol{\varepsilon}^e = \mathbf{C}\left(\boldsymbol{\varepsilon} - \boldsymbol{\varepsilon}^p\right) \tag{2}$$

where $\mathbf{C}$ is the matrix form of the fourth-order symmetric tensor that contains the elastic moduli E and ν.

In order to model the anisotropic plastic yielding of the AA7017-T73, the Yld2000-3d yield criterion [2] was chosen. The yield function is given by:

$$\phi\left[\boldsymbol{\sigma}, \bar{\varepsilon}_p, \dot{\bar{\varepsilon}}_p, T\right] = \bar{\sigma}[\boldsymbol{\sigma}] - k\left[\bar{\varepsilon}_p, \dot{\bar{\varepsilon}}_p, T\right] = 0 \tag{3}$$

where. $\bar{\sigma}$ is the equivalent stress and k is the isotropic hardening of the material that is defined as a combination of three terms that include Voce strain hardening, Johnson-Cook-based [4] strain rate hardening and thermal softening as,

$$k = k_v\left[\bar{\varepsilon}_p\right]\left\{1 + C\ln\left[\frac{\dot{\bar{\varepsilon}}_p}{\dot{\varepsilon}_0}\right]\right\}\left\{1 - \left(\frac{T - T_r}{T_m - T_r}\right)^m\right\} \tag{4}$$

where C and m are material constants, $\dot{\varepsilon}_0$ is the reference strain rate, and T_r and T_m are the reference and melting temperatures respectively. The strain hardening is defined as a Voce law,

$$\begin{aligned} k_v = \sigma_0 + Q_1\left(1 - \exp\left[-C_1\bar{\varepsilon}_p\right]\right) + \\ Q_2\left(1 - \exp\left[-C_2\bar{\varepsilon}_p\right]\right) \end{aligned} \tag{5}$$

where σ_0, Q_1, C_1, Q_2, C_2 are material constants.

The equivalent stress is expressed as a sum of two functions,

$$\bar{\sigma} = \frac{1}{2^{1/a}}\left(\phi'(\mathbf{s}') + \phi''(\mathbf{s}'')\right)^{\frac{1}{a}} \tag{6}$$

where

$$\begin{aligned} \phi'(\mathbf{s}') &= |s_1' - s_2'|^a \\ \phi''(\mathbf{s}'') &= |2s_2'' + s_1''|^a + |2s_1'' + s_2''|^a \end{aligned} \tag{7}$$

and s_1', s_2' and s_1'', s_2'' denote the principal values of the deviatoric stress tensors $\mathbf{s}'$ and $\mathbf{s}''$ given by the following linear transformations,

$$\begin{aligned} \mathbf{s}' &= \mathbf{L}'\boldsymbol{\sigma} \\ \mathbf{s}'' &= \mathbf{L}''\boldsymbol{\sigma} \end{aligned} \tag{8}$$

These tensors expressed as

$\mathbf{s}' = \{s_{xx}' \quad s_{yy}' \quad s_{zz}' \quad s_{xy}' \quad s_{yz}' \quad s_{zx}'\}^T$ and

$\mathbf{s}'' = \{s_{xx}'' \quad s_{yy}'' \quad s_{zz}'' \quad s_{xy}'' \quad s_{yz}'' \quad s_{zx}''\}^T$, while their zz components are independently defined through $s_{zz}' = -\left(s_{xx}' + s_{yy}'\right)$ and $s_{zz}'' = -\left(s_{xx}'' + s_{yy}''\right)$.

The linear transformations are specified through eight independent parameters α_k (for k from 1 to 8) associated with plane stress state anisotrpy, plus four parameters α_k (for k from 9 to 12) that are associated with out-of-plane shear stresses,

$$\mathbf{L}' = \frac{1}{3}\begin{bmatrix} 2\alpha_1 & -\alpha_1 & -\alpha_1 & 0 & 0 & 0 \\ -\alpha_2 & 2\alpha_2 & -\alpha_2 & 0 & 0 & 0 \\ 0 & 0 & 0 & 3\alpha_7 & 0 & 0 \\ 0 & 0 & 0 & 0 & 3\alpha_9 & 0 \\ 0 & 0 & 0 & 0 & 0 & 3\alpha_{10} \end{bmatrix} \tag{9}$$

$$\mathbf{L}'' = \frac{1}{9}\begin{bmatrix} L''_{11} & L''_{12} & L''_{13} & 0 & 0 & 0 \\ L''_{21} & L''_{22} & L''_{23} & 0 & 0 & 0 \\ 0 & 0 & 0 & 9\alpha_8 & 0 & 0 \\ 0 & 0 & 0 & 0 & 9\alpha_{11} & 0 \\ 0 & 0 & 0 & 0 & 0 & 9\alpha_{12} \end{bmatrix} \tag{10}$$

and

$$\begin{aligned} L''_{11} &= -2\alpha_3 + 2\alpha_4 + 8\alpha_5 - 2\alpha_6 \\ L''_{12} &= -4\alpha_4 + 4\alpha_6 + \alpha_3 - 4\alpha_5 \\ L''_{13} &= \alpha_3 + 2\alpha_4 - 4\alpha_5 - 2\alpha_6 \\ L''_{21} &= 4\alpha_3 - 4\alpha_4 - 4\alpha_5 + \alpha_6 \\ L''_{22} &= -2\alpha_3 + 8\alpha_4 + 2\alpha_5 - 2\alpha_6 \\ L''_{23} &= -2\alpha_3 - 4\alpha_4 + 2\alpha_5 + \alpha_6 \end{aligned} \tag{11}$$

Imposing $\alpha_9 = \alpha_{10} = \alpha_{11} = \alpha_{12} = 1$ provides satisfactory results in applications where the sheet material accommodates most deformation under plane stress conditions [5].

The direction of the plastic flow is given by an associated flow rule,

$$\dot{\boldsymbol{\varepsilon}}^p = \dot{\lambda}\frac{\partial \phi}{\partial \boldsymbol{\sigma}} \tag{12}$$

where $\dot{\lambda}$ is the plastic multiplier. The evolution equations of the internal hardening variables are

$$\dot{\bar{\varepsilon}}_p = \dot{\lambda} \tag{13}$$

$$\dot{T} = \frac{\chi\left[\dot{\bar{\varepsilon}}_p\right]}{\rho c_p}\boldsymbol{\sigma}\cdot\dot{\boldsymbol{\varepsilon}}^p \tag{14}$$

where χ is the Taylor-Quiney coefficient that evolves according to the strain rate

$$\chi[\bar{\varepsilon}_p] = \chi_0 \frac{\left(\dot{\bar{\varepsilon}}_p - \dot{\varepsilon}_0\right)^2\left(3\dot{\varepsilon}_a - 2\dot{\bar{\varepsilon}}_p - \dot{\varepsilon}_0\right)}{\left(\dot{\varepsilon}_a - \dot{\varepsilon}_0\right)^3} \tag{15}$$

where $\dot{\varepsilon}_0$ and $\dot{\varepsilon}_a$ are the limit strain rates for the isothermal and adiabatic domains, respectively.

3.2. Calibration procedure

The uniaxial yield stresses Y_0, Y_{45}, Y_{90}, and Lankford coefficients r_0 r_{45}, r_{90}, were not enough to identify the eight independent model parameters α_k (for k from 1 to 8). Typically additional equi-biaxial test data is used to identify such parameters. When these data are lacking, it is common practice [6] to assume that the r-ratio in equi-biaxial tension r_b is equal to unity and the yield stress is equal to that measured in the rolling direction $Y_0 = Y_b$. The yield exponent was chosen to be $a = 8$ since it is well established choice for materials with FCC crystal structures [7].

The seven constants of the hardening function (eq. (4)), $\{\sigma_0, Q_1, C_1, Q_2, C_2, C, m\}$ were identified through inverse modelling using LS-OPT optimisation software by LSTC. For such an optimisation, all tests shown in the previous section were simulated using an element size in the gauge length of 0.1 x 0.1 x 0.1 mm^3 applying the boundary conditions measured with the DIC technique. The constitutive model was implemented via user material subroutine in the non-linear finite element commercial code LS-DYNA. For the sake of simplicity the isothermal and adiabatic strain rate limits were set to $\dot{\varepsilon}_0 = 5{\cdot}10^{-3}$ s^{-1} and $\dot{\varepsilon}_a = 3$ s^{-1} respectively. The material constants are summarised in Table 3. Figure 3, 4 and 5 show the excellent agreement between the experimental and numerical stress-strain responses.

Table 2. Yield stresses and Lankford coefficients

Experimental data used for model calibration			
Y_0 (MPa)	Y_{45} (MPa)	Y_{90} (MPa)	Y_b (MPa)
434	400	413	434
r_0	r_{45}	r_{90}	r_b
0.5	0.84	0.61	1

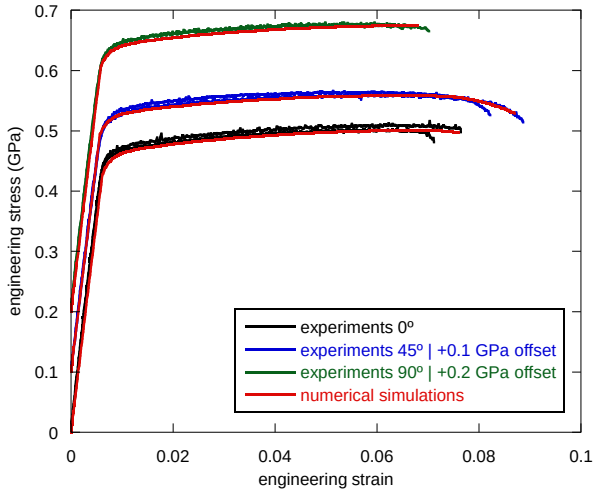

Figure 3. Stress-Strain curves obtained from uniaxial tensile experiments along three different directions (0º, 45º and 90º) compared with the corresponding numerical simulations.

Table 3. Material constants for the AA7017-T73

Physical constants and elastic moduli					
$\rho\ (\mathrm{kg/m^3})$	$c_p\ (\mathrm{J/kg^oC})$	$E\ (\mathrm{GPa})$	ν	χ_0	
2760.0	960.0	69.0	0.33	0.9	
Barlat Yld2000-3d yield surface with associated flow rule					
α_1	α_2	α_3	α_4	α_5	α_6	α_7	α_8
0.8582	1.0780	0.9022	1.0401	1.0258	0.9653	1.0537	1.2213
Voce strain hardening					
$s_0\ (\mathrm{MPa})$	$Q_1\ (\mathrm{MPa})$	C_1	$Q_2\ (\mathrm{MPa})$	C_2	
430.00	32.00	632.99	123.47	14.09	
JC strain rate hardening		JC thermal softening			
C	$\dot{\varepsilon}_0\ (\mathrm{s^{-1}})$	m	$\dot{\varepsilon}_a\ (\mathrm{s^{-1}})$	$T_r\ (\mathrm{^oC})$	$T_m\ (\mathrm{^oC})$
0.002	$5\cdot10^{-4}$	1.0	3.0	25.0	635.0

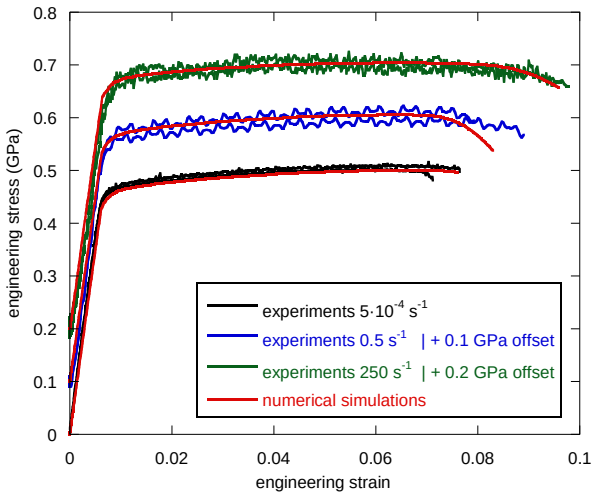

Figure 4. Stress-Strain curves obtained from uniaxial tensile experiments at three different strain rates compared with the corresponding numerical simulations.

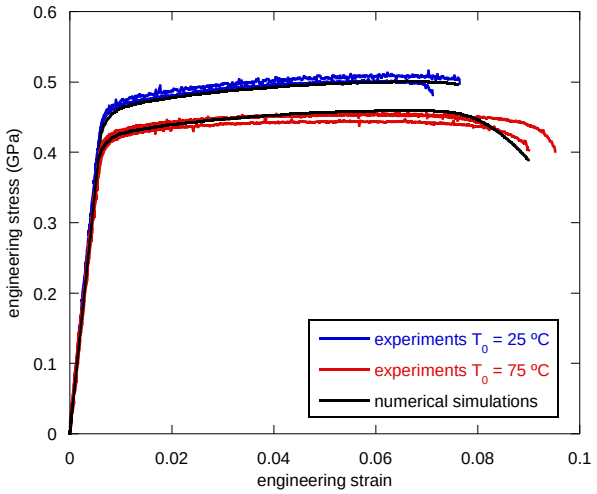

Figure 5. Stress-Strain curves obtained from uniaxial tensile experiments at 75ºC and room temperatures compared with the corresponding numerical simulations.

4. FRACTURE MODELLING

4.1. Failure criterion

In order to take into account the anisotropic fracture behaviour experimentally observed, an anisotropic version of the Cockcroft-Latham failure criterion [8] was proposed. Let us define the damage indicator as

$$D = \int_0^{\bar{\varepsilon}_p^f} \frac{1}{W_{cr}} \langle \hat{\sigma}_1 \rangle \, d\bar{\varepsilon}_p \tag{16}$$

where $\langle \bullet \rangle = \max[0, \bullet]$ are the Macaulay brackets and $\hat{\sigma}_1$ is the maximum principal stress of the stress tensor $\hat{\boldsymbol{\sigma}} = \mathbf{M}\boldsymbol{\sigma}$ being

$$\mathbf{M} = \begin{bmatrix} 1 & m_{12} & 0 & 0 & 0 & 0 \\ m_{12} & m_{22} & 0 & 0 & 0 & 0 \\ 0 & 0 & 1 & 0 & 0 & 0 \\ 0 & 0 & 0 & m_{44} & 0 & 0 \\ 0 & 0 & 0 & 0 & 1 & 0 \\ 0 & 0 & 0 & 0 & 0 & 1 \end{bmatrix} \tag{17}$$

This matrix contains the anisotropic constants m_{12}, m_{22} and m_{44}. According to eq. (16) when the plastic work reaches a critical value W_{cr} the material fails, i.e. $D = 1$. Note that when using $m_{12} = 0$, $m_{22} = 1$ and $m_{44} = 1$ the criterion collapses to the isotropic version of it and only one constant is necessary.

4.2. Calibration procedure

The parameters W_{cr}, m_{12}, m_{22}, m_{44} were identified using the results from the uniaxial tensile quasi-static experiments along the 0º, 45º and 90º directions. An optimization was performed using a derivative-free simplex algorithm (Matlab) which minimised the difference between the strains to fracture predicted by equation (16) with those extracted from the numerical simulations. The latter strains histories were extracted from the element with the highest equivalent plastic

strain and recorded until the displacement corresponding to fracture was reached. The final parameters of the anisotropic Cockroft-Latham failure criterion for the AA7017-T73 are given in Table 4.

Table 4. Calibrated parameters for the anisotropic Cockcroft-Latham failure criterion

Anisotropic Cockcroft-Latham failure criterion			
W_{cr} (MPa)	m_{12}	m_{22}	m_{44}
92.9	-1.9420	2.1065	0.8255

5. CONCLUSIONS

A series of uniaxial tensile tests on AA7017-T73 sheet specimens machined from different orientations with respect to the rolling direction was carried out at three loading rates and two different temperatures.

The experimental results revealed a high degree of anisotropy on both yield stress and plastic flow. In order to describe the anisotropy of the material, the Yld2000-3d yield criterion combined with an isotropic Voce hardening model were used. Finite element simulations showed that the plasticity model implemented as an user material subroutine provided accurate predictions.

The fracture strains measured from the simulations for different loading orientations showed large differences.

The anisotropic Cockcroft-Latham failure criterion was successfully used to describe such large differences in the fracture strains.

ACKNOWLEDGEMENTS

The financial support through the project BIA2011-24445 of the Secretariat of State for Research, Development and Innovation of the Spanish Ministry of Economy and Competitiveness is gratefully acknowledged. The authors would like to acknowledge the Laboratoire de Mécanique des Solides at École Polytechnique for letting them use their experimental facilities.

REFERENCES

[1] F. Barlat, J.C. Brem, J.W. Yoon, K. Chung, R.E. Dick, S.H. Choi, F. Pourboghrat, E. Chu and D.J. Lege, Plane stress yield function for aluminium alloy sheets, *International Journal of Plasticity* **19**, 1297-1319, 2003.

[2] M. Dunand, A.P. Maertens, M. Luo and D. Mohr, Experiments and modeling of anisotropic aluminum extrusions under multi-axial loading – Part I: Plasticity, *International Journal of Plasticity* **36**, 34-49, 2012.

[3] C.C. Roth, G. Gary and D. Mohr, Compact SHPB system for intermediate and high strain rate plasticity and fracture, *Experimental Mechanics* **55**, 1803-18011, 2015.

[4] G.R. Johnson and W.H. Cook, A constitutive model and data for metals subjected to large strains, high strain rates and high temperatures, *7th International Symposium on Ballistics, The Hague*, 541-547, 1983.

[5] M. Luo, M. Dunand and D. Mohr, Experiments and modeling of anisotropic aluminum extrusions under multi-axial loading – Part II: Ductile fracture, *International Journal of Plasticity* **32-33**, 36-58, 2012.

[6] O.S. Hopperstad, T. Børvik, T. Berstad, O.G. Lademo and A. Benalla, A numerical study on the influence of the Portevin–Le Chatelier effect on necking in an aluminium alloy, *Modelling and Simulation in Materials Science and Engineering* **15**, 747-772, 2007.

[7] R.W. Logan and W.F. Hosford, Upper bound anisotropic yield locus calculations assuming (1 1 1)-pencil glide, *International Journal of Mechanical Sciences* **22**, 419-430, 1980.

[8] M.G. Cockcroft and D.L. Latham, Ductility and workability of metals, *Journal of the Institute of Metals*, 33-39, 1968.